Shedding light on electronically doped perovskites

A.W. Stewart [a, b, *], A. Julien [b], D. Regaldo [b], P. Schulz [c], B. Marí Soucase [a], D.R. Ceratti [c, **],
P. López-Varo [b, ***]

[a] Universitat Politècnica de València, Camí de Vera, S/n, 46022, Valencia, Spain
[b] Insitute Photovoltaïque D'Ile de France, 18 Bd Thomas Gobert, 91120 Palaiseau, France
[c] CNRS, UMR 9006, IPVF, Institut Photovoltaïque D'Ile-de-France, 18 Boulevard Thomas Gobert, 91120 Palaiseau, France

ARTICLE INFO

ABSTRACT

Halide perovskites solar cells (PSCs) are making true on past promises, having reached power conversion efficiencies (PCEs) of 25.7% and long lifespans (>3000 h). Although stability has become the focus of research efforts, a significant number of researchers are still dedicated to further increasing cell efficiency. To push PCE any higher however, every element of the solar cell must be controlled and optimized. In the context of the recent advancements in halide perovskite doping, we analyse how and why doping can modify the PCE of PSCs. We find that optimal doping levels are highly dependent on carrier mobilities and device architecture, namely whether the hole- or electron-transport layer are on the front-side (illumination-side) of the device. More precisely, there are four regimes defined by carrier mobilities in which different physical processes are more, or less, important causing a change to the optimal doping level. When electron and hole mobilities are comparable, and diffusion lengths are not at least an order of magnitude larger than the perovskite film thickness, devices with the electron-transport layer on the front side (n-i-p) perform better with a p-doped perovskite, whereas devices with the hole-transport layer on the front side (p-i-n) perform better with an n-doped perovskite. The existence of these four regimes is especially pronounced for PSCs due to the very high absorption coefficients and rather low carrier mobilities in halide perovskites. We model the solar cell by employing a drift-diffusion simulation in SCAPS (a Solar Cell Capacitance Simulator) to provide a full rationale for the phenomenon and analyse the conditions under which this effect is significant. The findings presented here are based on the perovskite properties measured by multiple groups and are directed predominantly towards experimentalists working with devices.

© 2023 The Author(s). Published by Elsevier Ltd. This is an open access article under the CC BY license (http://creativecommons.org/licenses/by/4.0/).

1. Introduction

Since their inception, perovskite solar cells (PSCs) have experienced a meteoric growth in terms of power conversion efficiency (PCE), which now sits at a record 25.7% [1,2]. Research efforts have been driven by the attractive properties of tin- and lead-based halide perovskites, including their low cost [3], ability to self-heal [4–7], direct bandgap, high absorption coefficient, low binding energies [8,9], low defect densities [10], as well as large charge carrier diffusion lengths [11,12] and high charge carrier mobilities [13] for semiconductors made using solution-based deposition methods. Although research into PSCs has been booming over the past decade, halide perovskites also show great potential for other applications including LEDs, photodetectors, gamma-ray-detectors, and sensors. Their unique opto-electronic properties, which can be finely tuned using compositional engineering, make them a promising material for a wide range of applications.

Despite their elusive nature, electronically doped halide perovskites should be possible [14–20] and evidence of them grows daily [21–43]. While experimentally produced halide perovskites are usually considered intrinsic [30,44–46], it is likely that many are not, which is why we seek to better understand them in this paper. Indeed, a recent breakthrough in terms of PSC PCE was directly attributed to electronic doping of the perovskite [47]. Here we report the results of our investigations into the effect of doping halide perovskites, including identification of the conditions under

* Corresponding author.
** Corresponding author.
*** Corresponding author.
E-mail addresses: alste5@doctor.upv.es (A.W. Stewart), davide.ceratti@cnrs.fr (D.R. Ceratti), pilar.lopez-varo@ipvf.fr (P. López-Varo).

which a p-type or n-type perovskite layer is desirable, or not, in PSCs. Factors influencing the optimal doping level are also identified. We show that, under conditions of fixed illumination through the substrate, typical PSCs exhibit an optimal doping level depending on the device structure used. This effect occurs due to the asymmetric charge generation profile throughout the bulk of the perovskite absorber. Specifically, we find that n-i-p and p-i-n devices[1] perform better with a p-type or n-type perovskite absorber, respectively. This behaviour has been observed in recent experiments [47] and this paper sets out to propose the underlying theory. Fundamentally, the effect is a consequence of the charge carrier diffusion lengths being on the order of the absorber layer thickness, leading to potential charge extraction difficulties. Moreover, there are reports of diffusion lengths being shortened further by doping [48], which may provoke further charge recombination. Fabricating devices with optimized doping levels is especially important in the case of PSCs due to the high absorption coefficient of the perovskite layer, which highly localises photo-generated carriers. Adding to the complexity, the optimal doping level can be influenced by other perovskite properties, including charge carrier mobilities, defect densities, or layer thicknesses. By exploring the theoretical rationale for these effects, this work endeavours to establish guiding principles for the construction of superior PSCs.

Assuming it is possible to precisely control doping in perovskites, which despite difficulties appears to be the case, our intention is to determine why optimal doping levels arise, and how PCE can be maximised for common PSC architectures. To do so, the drift-diffusion modelling program SCAPS (a Solar Cell Capacitance Simulator) [49,50] was employed due to its proven track record of closely replicating experimental results [45,51,52]. In order to make simulations as physically realistic as possible, the input parameters used were carefully selected, by using a combination of literature values [53−63], in-house measurements and physical intuition (see Table S1).

To the best of our knowledge, there is little work on understanding electronically doped PSCs. Das et al. studied the effect of doping, photodoping and lateral bandgap variations on device relevant metrics using the Advanced Semiconductor Analysis (ASA) software [48]. Other studies have used simulations to optimise dopant concentration, however they were limited to a small range of values and conditions and tend not to explain the observed behaviour. For example, Raza et al. found that PCE was monotonically increasing as a function of acceptor concentration in p-i-n triple-cation-based PSCs [52]. Conversely, Patel et al. found that increasing the acceptor concentration in $CH_3NH_3SnI_3$-based PSCs led to a monotonical decrease in PCE of n-i-p devices [64]. Peña-Camargo et al. used SCAPS for one of the figures in their paper, and they found that PCE decreases as either acceptor or donor concentrations are increased [45]. Here we analyse a large set of dopant concentrations and properties, demonstrating how doping the perovskite layer can improve, or worsen, device performance depending on cell structure and perovskite film properties. Our results should be of significant interest to researchers working on PSCs because they establish simple guidelines for the improvement of devices. Following these can result in increases in PCE that could be highly impactful for already highly efficient devices. Finally, we provide an overview of the field, highlighting potential techniques

for the implementation of these principles as well as future avenues of research.

2. Results

To investigate PSCs with electronically doped perovskite absorbers, different parts of devices where systematically studied. To begin, the response of PCE to electronic doping of the perovskite absorber in realistic devices is made. In the second section, the impact of charge transport layers is explored. The third section is devoted to the influence of perovskite properties on optimal doping level. This includes the impact of absorption coefficient and device architecture, bulk and interfacial recombination rate, and carrier mobilities on the optimal electronic doping level in the perovskite layer.

2.1. Optimal doping levels in realistic devices

To model the electronic doping behaviour of standard lab-made devices we simulated the common n-i-p PSC structure, shown in Fig. 1a. Furthermore, we employed widely used electron-transport layer (ETL) and hole-transport layer (HTL) materials, namely TiO_2 and spiro-OMeTAD respectively. The material parameters used in the drift-diffusion simulations were carefully selected and can be found in Table S1. Throughout the study the thicknesses of the perovskite and charge transport layers were fixed at 400 nm and 50 nm respectively, which are comparable to the values found in the literature and in the high-performance devices made in our laboratory. Furthermore, to make sure our results were applicable to a range of halide perovskites, we used both the prototypical halide perovskite, $MAPbI_3$, and a triple-cation mixed-halide perovskite, $(MA_{0.17}FA_{0.83})_{0.95}Cs_{0.05}PbBr_{0.51}I_{2.49}$, which is often used in modern high-performance devices. To check the validity of our simulated parameters we compared them with reported experimental values of n-i-p devices using TiO_2 and spiro-OMeTAD, shown in Table 1, however without knowing the electronic doping level of the perovskite layer in the reported cells it is not possible to make a precise comparison. That said, the range with which PCE varies as a function of doping level should be applicable for a device with similar thickness and defect densities. Experimentally produced $MAPbI_3$-based devices appear to perform a few percentage points worse than those in our simulations. This could be explained by several factors including the experimentally produced films being slightly n-type and/or further loss channels in real devices such as defect-induced recombination, geometrical factors, and layer imperfections. On the other hand, experimentally produced triple-cation devices perform slightly better than predicted by our results which we attribute to the fact that we used the same bulk and interface defect densities for both halide perovskites, however there is evidence to suggest that the formamidinium cation promotes rapid defect self-healing [5] and cation mixing can suppress defect formation [15]. Another important point to make is that the values obtained in our simulations are lower than record-breaking PSCs which have PCEs of up to 25.7% [2]. This is due to the fact that they all used interfacial engineering to reduce non-radiative recombination and they employed slightly different perovskite compositions, making a direct comparison more difficult to be made [65−67]. Nevertheless, our results are applicable to these record PSC too as tuning the values of said parameters in our simulations still results in asymmetrical response of PCE to n-type or p-type doping (see figure S14).

Fig. 1b and c shows PCE as a function of doping level in the perovskite for $MAPbI_3$-based and triple-cation-based devices. The stars show carrier densities reported for these films, in some cases an arrow is used to signal a change in the measured electronic

---

[1] To increase the readability of our results, and be consistent with PSC literature, we use the terms n-i-p and p-i-n as shorthand for traditional PSCs where the perovskite absorber film is sandwiched between two selective contacts and illuminated via the electron- or hole-transport layer respectively.
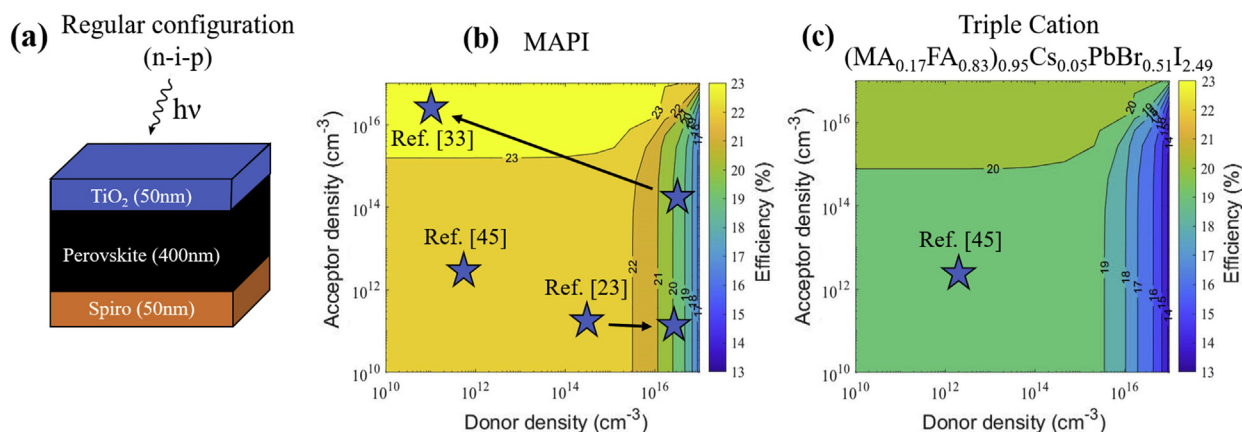
Fig. 1. (a) Simulated layer stack representing the structure of the n-i-p solar cell, with Spiro-OMeTAD as HTL and TiO$_2$ as ETL. Contour mappings of PCE as a function of donor and acceptor density in the (b) MAPbI$_3$ and (c) (MA$_{0.17}$FA$_{0.83}$)$_{0.95}$Cs$_{0.05}$PbBr$_{0.51}$I$_{2.49}$ perovskite layer. The parameters used in these simulations can be found in Table S1. Stars show experimentally measured carrier densities in MAPbI$_3$ and triple-cation mixed-halide perovskites. In some cases an arrow is used to represent the measured carrier densities before and after an electronic doping technique was used.

doping level before and after a technique changing the doping level was used [23,33]. However, these studies used different device structures meaning that a direct comparison of PCE cannot be made with our results. In Fig. 1b and c both devices show an asymmetrical response to p-type and n-type doping and perform best when the perovskite layer is p-doped with an acceptor density of N$_A$ = 10^{16} cm^{-3}. On the other hand, n-type doping appears to severely hamper performance. Although this behaviour was conserved across a range of absorber layer thicknesses, as thickness decreases the beneficial effect of doping becomes less pronounced since the diffusion length becomes larger with respect to the absorber thickness (see Figure S1). For devices based on both perovskites, there is approximately a 6% difference in PCE between a heavily p-doped and heavily n-doped absorber layer. Since it is not clear whether such high doping levels are physically obtainable, this value should be taken as an upper limit. Fig. 1b and c also show differences in doping sensitivity, which is how quickly PCE changes as the layer is doped. For both materials, an increase in PCE can be expected with p-doping, however in the case of the triple cation the maximum value of PCE is reached at a lower doping level.

These results raise several questions concerning the cause of this asymmetric doping behaviour, and whether it can be avoided. Our data suggests that the combination of high absorption coefficient and low carrier mobility creates a unique situation in halide perovskites where charge carriers are highly localised, and their diffusion lengths are comparable to the thickness of the perovskite films. This leads to hindered charge extraction which can be improved by electronic doping.

Table 1

Reported experimental values for PSCs with TiO$_2$/perovskite/spiro-OMeTAD architectures. The PCE of cells in this work correspond to those where the optimal doping level was implemented in the perovskite.

Perovskite composition	PCE	Reference
(MA$_{0.17}$FA$_{0.83}$)$_{0.95}$Cs$_{0.05}$PbBr$_{0.51}$I$_{2.49}$	20.7%	This work
(MA$_{0.17}$FA$_{0.83}$)$_{0.95}$Cs$_{0.05}$PbBr$_{0.51}$I$_{2.49}$	21.1%	Saliba et al. [68]
MA$_{0.15}$FA$_{0.81}$PbBr$_{0.45}$I$_{2.51}$	20.5%	Li et al. [69]
(MA$_{0.15}$FA$_{0.85}$)$_{0.95}$Cs$_{0.05}$PbBr$_{0.43}$I$_{2.57}$	19.76%	Zhao et al. [70]
MAPbI$_3$	23.9%	This work
MAPbI$_3$	20.2%	Zhang et al. [71]
MAPbI$_3$	19.7%	Ahn et al. [72]
MAPbI$_3$	19.0%	Noel et al. [73]

2.2. The impact of transport layers

To determine whether the optimal doping levels in Fig. 1 stem from properties of the charge transport layers, non-physical symmetric charge transport layers (see Table S2) were simulated. Both charge transport layers have the same density of states, doping levels and carrier mobilities. Furthermore, the same band offset is considered at the conduction and valence band at the ETL and HTL interfaces respectively. Under these conditions, key parameters of the charge transport layers were systematically varied in the n-i-p configuration to determine the effect on PCE doping response. Even in the case where the charge transport layers properties were symmetric an asymmetric doping level map, such as those in Fig. 1, arose. Moreover, this asymmetric behaviour was conserved for a range of doping concentrations, density of states, mobilities, and band offsets (see Figure S2). A more comprehensive analysis of the effect of changing the charge transport layers parameters on PCE can be found in the supporting information (see figure S2-S4). These findings suggest that the optimal doping level is dependent on the nature of the perovskite layer. For this reason, and in order to simplify the interpretation of results, symmetric charge transport layers (see Table S2) were used in the rest of the study.

2.3. The impact of bulk perovskite properties

2.3.1. Absorption and photogenerated carrier profile

In contrast to the properties of the charge transport layers we found that the profile of photogenerated carriers in the bulk perovskite, which depends on device architecture and optical properties, plays a critical role in identifying an optimal doping level. Fig. 2a and b shows how an optimal p-type or n-type doping can arise by illuminating the same device from the ETL (n-i-p) or HTL (p-i-n) side respectively. This is in agreement with what has been observed experimentally [47]. This asymmetric response to doping is driven mostly by changes in fill factor (see Figure S13). Furthermore, Fig. 2c shows how this behaviour disappears when a non-realistic constant generation profile is directly implemented. In this case, the generation profile is non-physical and cannot be straightforwardly related to an incident spectrum and power. For this reason, the total number of photogenerated carriers across the layer was adjusted to be the same as the value obtained by combining a Beer-Lambert Law with the AM1.5 spectrum. This
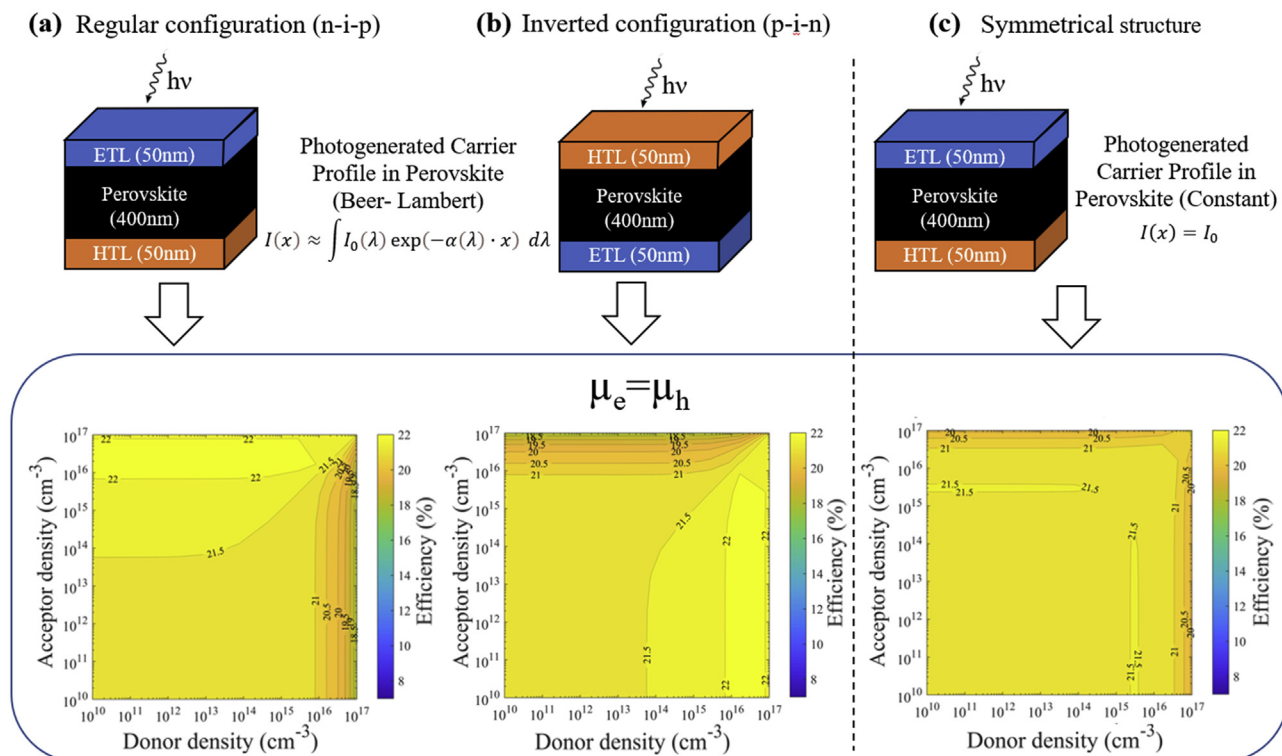
Fig. 2. PCE of PSCs using physically realistic parameters and symmetric charge transport layers that have the same band offset, carrier mobilities and doping level. (a) n-i-p structure (photogeneration from illumination on ETL side), (b) p-i-n structure (photogeneration from illumination on HTL side), (c) symmetrical structure (non-physical constant generation rate throughout the perovskite layer).

allows for the estimation of PCE by dividing the total power output by a 1 sun intensity. Generation profiles are represented in Figure S5.

To further probe the impact of different absorption profiles on optimal doping levels, a range of generation functions were used to simulate photogenerated carriers being created at different depths. These square functions, seen in Fig. 3a, while non-physical when considered independently, can model physically realistic absorption profiles when linear combinations of these functions are used. Fig. 3b shows diagrammatically how a Beer-Lambert absorption can be modelled in the perovskite layer by adding a weighting factor to each function. In the limit where the width of the square functions go to zero, any incident spectra can be modelled exactly.

Fig. 3c shows the difference in PCE of highly n-doped, with $N_D = 10^{17} cm^{-3}$, and highly p-doped, with $N_A = 10^{17} cm^{-3}$, devices. Doping level maps for each square function can be found in Figure S8. Intuitively, if charges are generated near an interface, it is easier for them to reach it. If photogenerated carriers are created near the HTL (at 0 nm) they will reach it more efficiently than the ETL (at 400 nm) since the layer thickness is of the same order as the diffusion length of the charges. In addition, band bending, and the associated electric field, can also promote the separation of charges and their transportation. Doping the perovskite layer localises the band bending at one extremity of the layer and flattens it at the other (see Figure S6), meaning that electric field is also localised (see Figure S7). Since both electric field and photogenerated charge carriers are localised, their respective locations are key for optimising charge carrier extraction. Hence by altering the position of the photogenerated carriers from the HTL-side (as it would be in a p-i-n configuration) to the ETL side (as it would be in an n-i-p

configuration), the preference for n-doping turns into a preference for p-doping.

Furthermore, in p-doped materials, the minority carriers (governing charge transport) are electrons while in n-doped materials they are holes. Considering a p-i-n configuration, if the intrinsic material becomes p-doped, the minority carriers, which are electrons, must travel through the entire perovskite layer to reach the ETL while if the material is n-doped, the minority carriers, which are the holes, can easily reach the HTL on the front. This phenomenon, coupled with the localised electric field, explains why PCE is higher when charges are generated near the HTL if the material is n-doped than when it is p-doped as we can see in the leftmost point of Fig. 3c. Interestingly these effects remain true even when introducing traps in the layer, increasing interface or bulk defects, or lowering carrier mobility (details are provided in Table S3).

As carriers are generated closer to the centre of the layer, the effect diminishes, until it vanishes completely at the centre (at 200 nm), and no doping type is preferred. Moving further to the right, the reasoning can be inverted and it becomes more favourable to be p-doped since the electrons, which are the minority carriers, reach the ETL (at 400 nm) more easily.

To probe the non-linear recombination effects that depend on charge concentrations, we simulated solar cells with different exponential decay generation profiles, which correspond physically to absorption coefficients for a given wavelength (i.e. monochromatic light) when illuminated from either the ETL or HTL side. Here again the synthetic generation profiles were weighted to the total generation rate obtained from a Beer-Lambert Law combined with the AM1.5 spectrum. Fig. 3d shows the difference in PCE
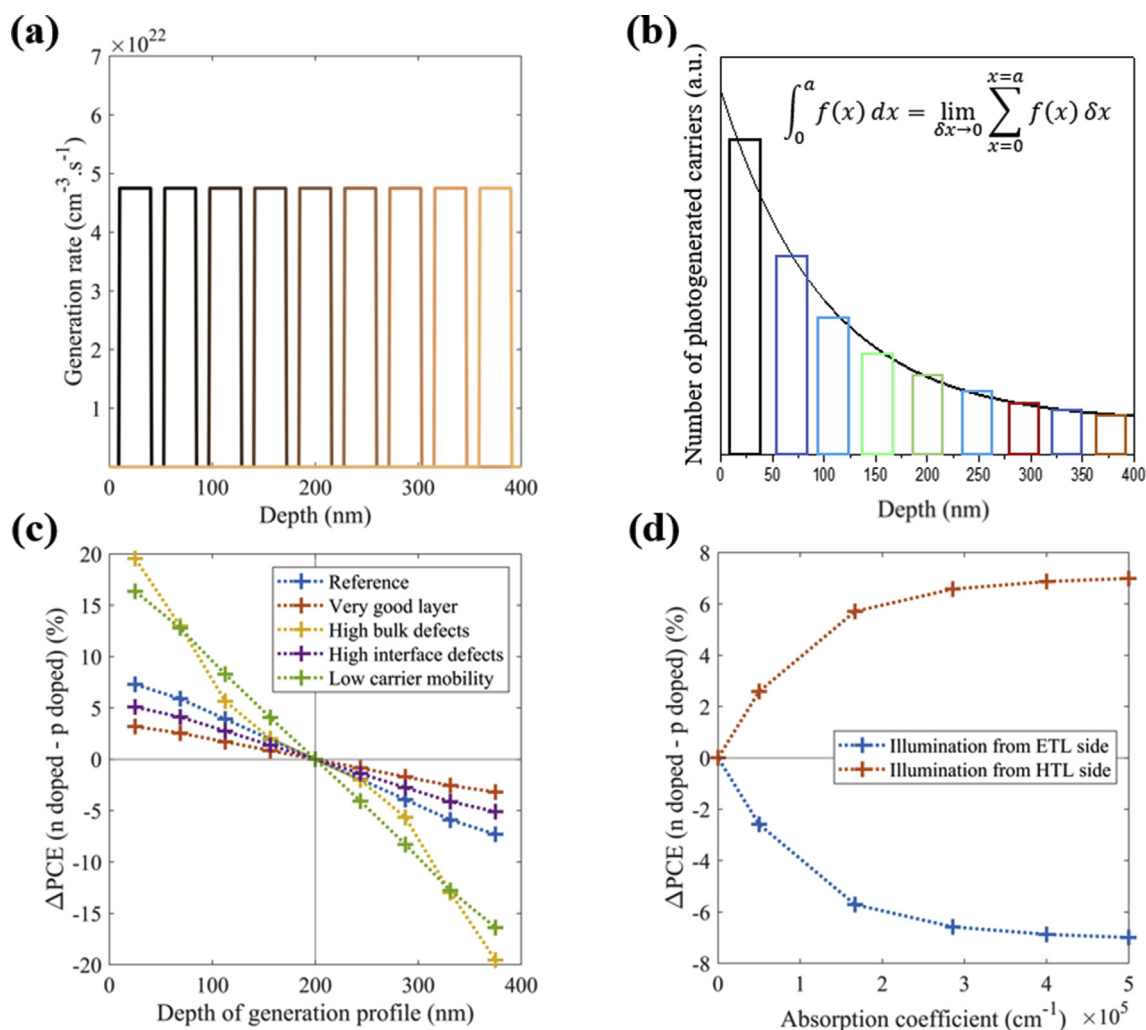
Fig. 3. (a) Square (30 nm wide) photogenerated carrier distributions used for the simulations. Depth scale starts from HTL interface (0 nm) to the ETL interface (400 nm) (b) Diagrammatic explanation for how physically realistic carrier distributions can be modelled with square functions. (c) Resulting power difference between p-type perovskite ($N_a = 10^{17} cm^{-3}$) and n-type perovskite ($N_d = 10^{17} cm^{-3}$) when using the square functions in (a) as the photogenerated carrier profiles. HTL is at the front (left) and ETL is at the back (right). Several configurations of defects and mobilities are simulated. (d) Power difference between p-type perovskite ($N_A = 10^{17} cm^{-3}$) and n-type perovskite ($N_D = 10^{17} cm^{-3}$) as a function of absorption coefficient for both n-i-p and p-i-n configurations. Associated data is in supporting information Tables S2 and S3, Figures S8 and S9.

between a heavily n-doped and p-doped device as a function of the absorption coefficient. The higher the absorption coefficient, the more photogeneration is localised near the front interface. This results in an increasingly desirable p-doping when illuminated via the ETL (blue in Fig. 3d) or n-doping when illuminated via the HTL (orange in Fig. 3d). When the absorption coefficient tends to zero, no effect can be seen since charges are generated equally throughout the perovskite layer.

These results demonstrate why the distance between the photogenerated carriers and the space-charge region is important in PSCs, an effect that has been observed previously by other authors [69]. Moreover, these results show that doping is key for achieving high efficiencies when materials with high absorption coefficients are used, assuming that the charge's diffusion lengths are not at least an order of magnitude larger than the film themselves (as is the case in Si and GaAs).

2.3.2. Bulk and interface recombination

In the previous section we showed how an optimal doping level can arise due to non-uniform photogeneration, with most carriers being created near the front side of the perovskite layer. Moreover,

electron-hole pair separation can also be hindered if the doping localises the band bending at the back interface (see Figures S6 and S7). In this context, charge carrier transport and recombination play key roles. To study this further, we investigated the effect of changing defect densities which correspond to neutral recombination centres inside the bulk of the perovskite layer and at the interfaces with the charge transport layers (details can be found in Table S3, Figures S10 to S14).

Fig. 3c shows that the configuration with the best transport properties (low bulk and interface defects, red) not only has the lowest PCE difference between heavily n-doped and p-doped cells, but also the lowest dependence on generation depth. Conversely, having a high defect density of 10^{17} cm^{-3} in the perovskite layer (yellow) leads to large variations, which are more sensitive to generation location, in optimal doping level. For instance, if the generation is on the HTL side (low depth values) and the doping is p-type, the separation of carriers relies almost exclusively on diffusion, meaning that electrons must diffuse across the width of the absorber to reach the ETL. Naturally, a perovskite layer with high defect density is highly detrimental in this case. Similarly, when lower mobilities are considered (both electron and hole

mobility lowered to 0.1 cm^2/V/s), a similarly strong dependence on doping and generation profile is observed.

To probe the impact of bulk perovskite defects on optimal doping level, we simulated the cells in Fig. 2 with both low (10^{10} cm^{-3}) and high (10^{17} cm^{-3}) defect densities. Independent of defect density, devices illuminated from the ETL side had an optimal p-doping level and those illuminated from the HTL side an optimal n-doping level. Furthermore, an intrinsic layer was preferred when generation rate was constant irrespective of the defect density. Across all three cases, increasing the bulk defect density reinforced the benefits of doping because it increased the probability of recombination, negatively impacting transport properties and the effective diffusion length of photogenerated carriers. This exacerbates the difficulty in extracting the minority carriers. Doping level maps of J_{SC}, V_{OC}, and FF can be found in Figures S11 to S13.

We also investigated the role that interface defects between the perovskite and the charge transport layers played in determining the optimal doping level. We found that the optimal doping level was conserved irrespective of the interfacial recombination rate (see Figure S14), although there was a slight decrease in PCE at high dopant densities due to the increased recombination.

2.3.3. The impact of asymmetrical carrier mobilities

Until now, equal electron and hole mobilities have been considered in the perovskite layer, however in real devices hole mobilities tend to be lower than their electron counterparts. Moreover, we found that the value of charge carrier mobilities was critical in determining the optimum doping level. In two cases, when the ratio of the charge carrier mobilities is very small or large, the optimal doping level dependence on photogenerated carrier profile can disappear completely. To investigate the effect of having asymmetric electron-hole mobilities, simulations were carried out using a constant electron mobility of 1 cm^2/V/s, while hole mobility was varied an order of magnitude from 1 to 0.1 cm^2/V/s.

Fig. 4a, similarly to Fig. 3d, shows that the more carriers that are generated close to the edge of the absorber layer, the more it becomes advantageous to be doped. This trend is persistent throughout all mobility conditions. However, as hole mobility is

decreased, the PCE difference between n- and p-doped devices are downshifted. This leads to a limiting case where for a given absorption coefficient and low enough hole mobility it is always preferable for the perovskite to be p-doped since this makes the holes the majority carriers and therefore improves their transport.

Another interesting finding is that for each set of mobilities there exists an absorption coefficient where there is no optimal doping level. The perovskite layer thickness, which is constant in this study, is also likely to play a role in this effect. For example, when the hole mobility is 0.1 cm^2/V/s no doping type is preferred when absorption coefficient is approximately 1.2×10^5 cm^{-1}. This demonstrates an inner balance occurring between carrier mobility and photogeneration profile which can lead to several physical regimes depending on whether carrier mobilities are comparable or not.

Fig. 4b identifies the separate physical regimes determined by carrier mobilities. This figure was obtained by combining several doping maps with different device structures and bulk defect densities (see Figure S15). We find that when there is a very strong mobility asymmetry there are regions where it is always better to have a certain doping type. On the other hand, in the central area where both mobilities are comparable, the optimal doping level depends on the profile of the photogenerated carriers. Fig. 4b also shows two different bulk defect densities in the perovskite layer. As reported in the previous section, bulk defect densities increase the sensitivity of PCE to doping. This manifests itself in Fig. 4c as an expansion of the area where doping level is dependent on photogenerated carrier profile, meaning that higher asymmetries in mobilities must be reached before doping level is insensitive to device configuration.

3. Methods and insights for electronically doping PSCs

In order to exploit the results presented so far, this section explores the available experimental techniques for doping halide perovskites. Here we review different approaches for electronically doping perovskites, in order to obtain elevated numbers of free charges in the material. These include the intrinsic (i.e. non-stochiometric films) and extrinsic (i.e. via impurities) doping of
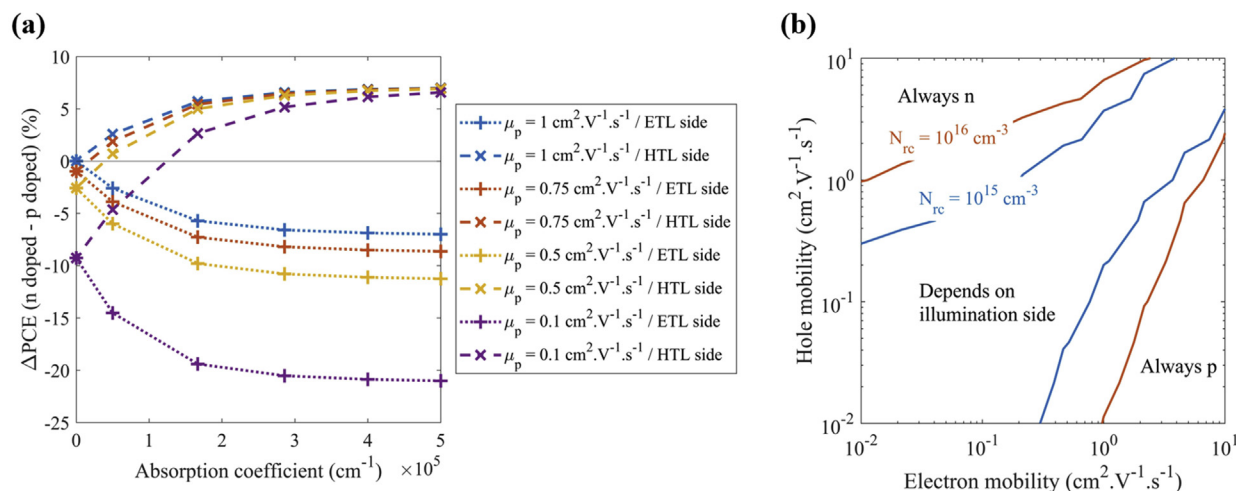

Fig. 4. (a) Difference in PCE between simulated cells with a p-type perovskite (Na = 10^{17} cm^{-3}) and n-type perovskite (Nd = 10^{17} cm^{-3}) as a function of perovskite absorption coefficient. n-i-p configuration corresponds to the doted lines and plus signs, whereas p-i-n configuration corresponds to dashed lines and x signs. (b) The three limiting cases defined by carrier mobilities when diffusion lengths are not at least an order of magnitude larger than the perovskite layer. Associated data in supporting information Figure S15. When there is a large difference between carrier mobilities, it is best for the carrier with the reduced mobility to be made the majority carrier. This is independent of the device architecture used. However, when mobilities are comparable, whether p-doping or n-doping should be used depends on device architecture and illumination conditions. Increasing bulk defect density in the perovskite layer from 10^{15} cm^{-3} to 10^{16} cm^{-3} results in a broadening of this region.

halide perovskites as well as remote doping through charge transfer from adjacent layers.

Intrinsic doping of perovskites has been explored from a theoretical point of view [14–17] and reported experimentally [21,22,33,37–40]. Density functional theory (DFT) calculations indicate the possibility of making a range of compositions more or less p- or n-type by controlling growth conditions. Such compositions include $MAPbI_3$ [14], $FAPbI_3$ [15], $MAPbBr_3$ [16] and $MASnI_3$ [17]. In the case of $FAPbI_3$ and $MAPbI_3$ it should be possible to produce either n- or p-type films by growing them in Pb-rich or Pb-poor conditions respectively [14,15], however $MAPbBr_3$ and $MASnI_3$ films tend towards being p-type [16,17].

In terms of the experimental evidence, several studies report p-type behaviour in tin-based perovskites which is attributed to the propensity of tin to oxidise [21,22,40]. Many studies have also shown a p-type to n-type phase transition by changing the stoichiometry of the precursor and several perovskite homojunctions have been fabricated using this property [35,36]. Wang et al. found that changing the MAI to PbI_2 ratio in the $MAPbI_3$ precursor solution from 0.3 to 1.7 resulted in p-type or n-type films with carrier concentrations of up to 4×10^{16} cm^{-3} holes and 3.5×10^{18} cm^{-3} electrons respectively [33]. Su et al. reported similar findings for $MAPbBr_3$ [38]. There is also evidence that suggests there exists the possibility of intrinsically doping films after their synthesis. Zohar et al. carried out a post-processing treatment of $MAPbI_3$ using I_2 vapour [37]. They found that the post-processing method increased conductivity by an order of magnitude, altered the diffusion lengths of the carriers and led to a 150 mV increase in the work function which they attribute to the film becoming p-type. Furthermore, Song et al. exploited the volatile nature of MA in order to prepare more or less n-type films by controlling the annealing temperature [39].

Similarly to intrinsic doping, extrinsic doping has been explored from both theoretical [16,18–20] and experimental [23–29,41–43] points of view. First-principles calculations suggest that $MAPbI_3$ can be made p-type or n-type depending on the group that the dopant belongs to and the position it occupies in the lattice [18]. That said, while the production of p-type $MAPbI_3$ via doping with group IA, IB and VIA elements under I-rich/Pb-poor growth should be straight forward, n-type doping requires non-equilibrium growth conditions [18]. It is noteworthy that $MAPbBr_3$ is much more difficult to dope extrinsically since intrinsic defects such as Pb and Br vacancies that compensate extrinsic doping are very stable [16]. In terms of inorganic perovskites, some DFT calculations support the claim that p- or n-type $CsPbI_3$ can be achieved through group IIIA and VA doping [19], however intrinsic defects were not considered in this study and they may play an important role [74].

In a number of experiments a range of elements have been claimed to act as dopants or acceptors in perovskites [74]. This may not be so straightforward as appears and care should be taken when adding extrinsic dopants into the precursor solution because it is possible to inadvertently change the crystallization kinetics, surface chemistry, and/or the AX/PbX_2 ratio which directly impacts the growth conditions of intrinsic defects. Senocrate et al. reported on the p-type behaviour of halide perovskites when interacting with oxygen which they attributed to the O^{2-} substituting I^- or sitting on interstitial sites [41]. Ag has also been proposed as an acceptor dopant with p-type $MAPbI_3$ [26] and $CsPbBr_3$ [27] being reported. Several results also suggest that the hole density in p-type $MAPbI_3$ can be controlled through the inclusion of NaI and RbI in the precursor solution [42,43]. With reference to n-type doping, Huang et al. varied the electron density in $MAPbI_3$ from 7.2×10^{14} cm^{-3} up to 8.3×10^{16} cm^{-3} by substituting Pb^{2+} with Sb^{3+} [23]. In an alternative approach Abdelhady et al. and Meng et al. increased carrier density up to 2×10^{16} cm^{-3} by doping with

$MAPbBr_3$ with Bi^{3+} [24,25]. Li has also shown potential, with n-type $MAPbI_3$ [28] and $CsPbBr_3$ [29] being reported. In fact, it is plausible that many reported PSCs have unknowingly been doped with Li since it is often used to dope the spiro-OMeTAD layer and it may be able to diffuse into the perovskite from the HTL [75].

Several groups have reported an apparent substrate-dependent shift in the Fermi level position in the perovskite film which could be associated with charge transfer or remote doping [30–32,34]. The fact that changing the doping of a substrate can alter the Fermi level position deep in the bulk of $MAPbI_3$ films, which are grown on top, suggests a low intrinsic carrier density in the perovskite film [44,76]. Similar effects were observed for triple-cation lead bromide films on a range of substrates, for which the work function of the halide perovskite was monotonically decreasing as a function of the substrate's work function [34]. Noel et al. took a different approach, pre-treating the substrate with a fluorinated ionic liquid to make the perovskite n-type [77]. These results highlight the potential for using substrates as a means of controlling the band alignment in PSCs.

Molecular doping, i.e. the transfer of charge between an organic molecular species and an adjacent semiconductor, has also developed into a significant field of study for the doping of perovskites [78–84]. For molecular doping to work, the lowest unoccupied molecular orbital (LUMO) or highest occupied molecular orbital (HOMO) of the dopant must be above the conduction band or below the valence band of the perovskite for n- or p-doping respectively [74].

An important factor to consider when implementing these techniques is the effect that electronical doping can have on device stability. In some cases, improving the doping level of the perovskite can improve lifespan of the device [47] however this is not always the case [85]. To our best knowledge, there is no clear consensus on the relationship between large families of electronic doping techniques and device stability. However, this knowledge, in combination with the findings presented here, could be invaluable to some device makers. For this reason, we highlight this as an area which merits further investigation.

4. Conclusion

In this work we analyse the processes driving an optimal doping level in PSCs and provide tools for improving devices. Optimal doping levels are shown to originate in the properties of the perovskite layer itself, due to the relatively low carrier mobilities and high absorption coefficients of halide perovskites. Varying the type of doping modifies the nature of the space charge region created at the charge transport layer/perovskite junction, which can hinder or promote the extraction of charge. The high absorption coefficients of halide perovskites lead to a strong localisation of photogenerated carriers on the front side of the absorber layer, which is why the choice of an n-i-p or p-i-n structure generally dictates whether p-type or n-type doping is optimal. This effect has been overlooked in PSCs because in other semiconductors commonly used in photovoltaic applications, such as Si and GaAs, charge mobilities are normally large enough that diffusion lengths are orders of magnitude longer than the absorber thickness. This is not the case for halide perovskites, and it leads to a lower charge extraction efficiency.

We find that the relationship between electron and hole carrier mobilities has a critical impact on the optimal doping level. Specifically, we find that there are four regimes depending on values of electron and hole mobilities. Firstly, when they are both high enough, so that charge carrier diffusion lengths are much larger than the absorber thickness, optimal doping level is insensitive to device structure. However, the remaining three cases, which are

more pronounced in PSCs due to the lower mobilities, occur when electron mobility is either much larger, equal to, or much smaller than hole mobility. In the cases where mobilities are very different, devices will perform best when the majority carriers are the ones with lower mobilities. However, in the case where mobilities are comparable, the optimal doping level is a function of device architecture, namely whether the ETL and HTL are on the front- and back-side or vice versa. Having established the profile of photogenerated carriers as the source of the optimal doping level, we investigate the impact of perovskite properties on said effect. Bulk defects in the perovskite are shown to be important in exaggerating the effect since they impede charge transport. Absorber thickness is also important because the optimal doping levels originate from the fact that diffusion lengths are on the order of the film thickness. Lastly, any increases in absorption coefficient will also exacerbate the impact of doping since it will increase the localisation of photogenerated carriers.

For these reasons, device makers should be aware that PCE may be fundamentally limited for a given device configuration depending on the deposition conditions and perovskite composition used. For example, this should be considered when using non-stoichiometric growth conditions or perovskites with a tendency to self-dope, such as tin-based ones [21,22,40]. The results presented here contribute to the development of a better understanding of electronic doping in PSCs as well as provide avenues of research for the development of future high-performance devices.

Funding

Data availability

The raw data required to reproduce these findings is available in the supporting information. The processed data required to reproduce these findings cannot be shared at this time due to technical or time limitations.

Declaration of competing interest

The authors declare that they have no known competing financial interests or personal relationships that could have appeared to influence the work reported in this paper.

Data availability

Data will be made available on request.

Appendix A. Supplementary data

Supplementary data to this article can be found online at https://doi.org/10.1016/j.mtchem.2023.101380.

References

[1] A. Kojima, K. Teshima, Y. Shirai, T. Miyasaka, Organometal halide perovskites as visible-light sensitizers for photovoltaic cells, J. Am. Chem. Soc. 131 (2009) 6050–6051, https://doi.org/10.1021/ja809598r.

[2] Best Research-Cell Efficiency Chart | Photovoltaic Research | NREL, (n.d.). https://www.nrel.gov/pv/cell-efficiency.html (accessed October 6, 2022).

[3] H.J. Snaith, Perovskites: the emergence of a new era for low-cost, high-efficiency solar cells, J. Phys. Chem. Lett. 4 (2013) 3623–3630, https://doi.org/10.1021/jz4020162.

[4] D.R. Ceratti, Y. Rakita, L. Cremonesi, R. Tenne, V. Kalchenko, M. Elbaum, D. Oron, M.A.C. Potenza, G. Hodes, D. Cahen, Self-healing inside APbBr3 halide perovskite crystals, Adv. Mater. 30 (2018), 1706273, https://doi.org/10.1002/ADMA.201706273.

[5] D.R. Ceratti, A.V. Cohen, R. Tenne, Y. Rakita, L. Snarski, N.P. Jasti, L. Cremonesi, R. Cohen, M. Weitman, I. Rosenhek-Goldian, I. Kaplan-Ashiri, T. Bendikov, V. Kalchenko, M. Elbaum, M.A.C. Potenza, L. Kronik, G. Hodes, D. Cahen, The pursuit of stability in halide perovskites: the monovalent cation and the key for surface and bulk self-healing, Mater. Horiz. 8 (2021) 1570–1586, https://doi.org/10.1039/D1MH00006C.

[6] D.R. Ceratti, R. Tenne, A. Bartezzaghi, L. Cremonesi, L. Segev, V. Kalchenko, D. Oron, M.A.C. Potenza, G. Hodes, D. Cahen, Self-healing and light-soaking in MAPbI 3 : the effect of H 2 O, Adv. Mater. (2022), https://doi.org/10.1002/adma.202110239.

[7] S. Aharon, D.R. Ceratti, N.P. Jasti, L. Cremonesi, Y. Feldman, M.A.C. Potenza, G. Hodes, D. Cahen, 2D Pb-halide perovskites can self-heal photodamage better than 3D ones, Adv. Funct. Mater. 32 (2022), https://doi.org/10.1002/adfm.202113354.

[8] A. Miyata, A. Mitioglu, P. Plochocka, O. Portugall, J.T.W. Wang, S.D. Stranks, H.J. Snaith, R.J. Nicholas, Direct measurement of the exciton binding energy and effective masses for charge carriers in organic-inorganic tri-halide perovskites, Nat. Phys. 11 (2015) 582–587, https://doi.org/10.1038/nphys3357.

[9] V. D'Innocenzo, G. Grancini, M.J.P. Alcocer, A.R.S. Kandada, S.D. Stranks, M.M. Lee, G. Lanzani, H.J. Snaith, A. Petrozza, Excitons versus free charges in organo-lead tri-halide perovskites, Nat. Commun. 5 (2014), https://doi.org/10.1038/ncomms4586.

[10] A. Musiienko, D.R. Ceratti, J. Pipek, M. Brynza, H. Elhadidy, E. Belas, M. Betušiak, G. Delport, P. Praus, Defects in hybrid perovskites: the secret of efficient charge transport, Adv. Funct. Mater. 31 (2021), https://doi.org/10.1002/adfm.202104467.

[11] M.J.P. Alcocer, T. Leijtens, L.M. Herz, A. Petrozza, H.J. Snaith, Electron-hole diffusion lengths exceeding trihalide perovskite absorber, Science 342 (2013) 341–344, https://doi.org/10.1126/science.1243982.

[12] G. Xing, N. Mathews, S. Sun, S.S. Lim, Y.M. Lam, M. Graïzel, S. Mhaisalkar, T.C. Sum, Long-range balanced electron-and hole-transport lengths in organic-inorganic CH3NH3PbI3, Science 342 (2013) 344–347, https://doi.org/10.1126/science.1243167.

[13] L.M. Herz, Charge-carrier mobilities in metal halide perovskites: fundamental mechanisms and limits, ACS Energy Lett. 2 (2017) 1539–1548, https://doi.org/10.1021/acsenergylett.7b00276.

[14] W.J. Yin, T. Shi, Y. Yan, Unusual defect physics in CH3NH3PbI3 perovskite solar cell absorber, Appl. Phys. Lett. 104 (2014), https://doi.org/10.1063/1.4864778.

[15] N. Liu, C.Y. Yam, First-principles study of intrinsic defects in formamidinium lead triiodide perovskite solar cell absorbers, Phys. Chem. Chem. Phys. 20 (2018) 6800–6804, https://doi.org/10.1039/c8cp00280k.

[16] T. Shi, W.J. Yin, F. Hong, K. Zhu, Y. Yan, Unipolar self-doping behavior in perovskite CH3NH3PbBr3, Appl. Phys. Lett. 106 (2015), https://doi.org/10.1063/1.4914544.

[17] D. Meggiolaro, D. Ricciarelli, A.A. Alasmari, F.A.S. Alasmary, F. De Angelis, Tin versus lead redox chemistry modulates charge trapping and self-doping in tin/lead iodide perovskites, J. Phys. Chem. Lett. 11 (2020) 3546–3556, https://doi.org/10.1021/acs.jpclett.0c00725.

[18] T. Shi, W. Yin, Y. Yan, Predictions for p-type CH 3 NH 3 PbI 3 perovskites, J. Phys. Chem. C 118 (2014) 25350–25354, https://doi.org/10.1021/jp508328u.

[19] Y. Chen, H. Jing, F. Ling, W. Kang, T. Zhou, X. Liu, W. Zeng, Y. Zhang, L. Qi, L. Fang, M. Zhou, Tuning the electronic structures of all-inorganic lead halide perovskite CsPbI3 via heterovalent doping: a first-principles investigation, Chem. Phys. Lett. 722 (2019) 90–95, https://doi.org/10.1016/j.cplett.2019.02.050.

[20] W. Chen, H. Chen, G. Xu, R. Xue, S. Wang, Y. Li, Y. Li, Precise control of crystal growth for highly efficient CsPbI2Br perovskite solar cells, Joule 3 (2019) 191–204, https://doi.org/10.1016/j.joule.2018.10.011.

[21] Y. Takahashi, H. Hasegawa, Y. Takahashi, T. Inabe, Hall mobility in tin iodide perovskite CH3NH3SnI 3: evidence for a doped semiconductor, J. Solid State Chem. 205 (2013) 39–43, https://doi.org/10.1016/j.jssc.2013.07.008.

[22] M.A. Haque, L.H. Hernandez, B. Davaasuren, D.R. Villalva, J. Troughton, D. Baran, Tuning the thermoelectric performance of hybrid tin perovskites by air treatment, Adv. Energy Sustain. Res. 1 (2020), 2000033, https://doi.org/10.1002/aesr.202000033.

[23] L. Huang, S. Bu, D. Zhang, R. Peng, Q. Wei, Z. Ge, J. Zhang, Schottky/p-n cascade heterojunction constructed by intentional n-type doping perovskite toward efficient electron layer-free perovskite solar cells, Sol. RRL 3 (2019) 1–13, https://doi.org/10.1002/solr.201800274.

[24] A.L. Abdelhady, M.I. Saidaminov, B. Murali, V. Adinolfi, O. Voznyy, K. Katsiev, E. Alarousu, R. Comin, I. Dursun, L. Sinatra, E.H. Sargent, O.F. Mohammed, O.M. Bakr, Heterovalent dopant incorporation for bandgap and type engineering of perovskite crystals, J. Phys. Chem. Lett. 7 (2016) 295–301, https://doi.org/10.1021/acs.jpclett.5b02681.

[25] R. Meng, G. Wu, J. Zhou, H. Zhou, H. Fang, M.A. Loi, Y. Zhang, Understanding the impact of bismuth heterovalent doping on the structural and photophysical properties of CH 3 NH 3 PbBr 3 halide perovskite crystals with near-IR photoluminescence, Chem. Eur J. 25 (2019) 5480–5488, https://doi.org/10.1002/chem.201805370.

[26] Q. Chen, L. Chen, F. Ye, T. Zhao, F. Tang, A. Rajagopal, Z. Jiang, S. Jiang, A.K.Y. Jen, Y. Xie, J. Cai, L. Chen, Ag-incorporated organic-inorganic perovskite films and planar heterojunction solar cells, Nano Lett. 17 (2017) 3231–3237, https://doi.org/10.1021/acs.nanolett.7b00847.

[27] S. Zhou, Y. Ma, G. Zhou, X. Xu, M. Qin, Y. Li, Y.J. Hsu, H. Hu, G. Li, N. Zhao, J. Xu, X. Lu, Ag-doped halide perovskite nanocrystals for tunable band structure and efficient charge transport, ACS Energy Lett. 4 (2019) 534–541, https://doi.org/10.1021/acsenergylett.8b02478.

[28] Z. Fang, H. He, L. Gan, J. Li, Z. Ye, Understanding the role of lithium doping in reducing nonradiative loss in lead halide perovskites, Adv. Sci. 5 (2018) 1–6, https://doi.org/10.1002/advs.201800736.

[29] Q. Jiang, M. Chen, J. Li, M. Wang, X. Zeng, T. Besara, J. Lu, Y. Xin, X. Shan, B. Pan, C. Wang, S. Lin, T. Siegrist, Q. Xiao, Z. Yu, Electrochemical doping of halide perovskites with ion intercalation, ACS Nano 11 (2017) 1073–1079, https://doi.org/10.1021/acsnano.6b08004.

[30] P. Schulz, L.L. Whittaker-Brooks, B.A. Macleod, D.C. Olson, Y.L. Loo, A. Kahn, Electronic level alignment in inverted organometal perovskite solar cells, Adv. Mater. Interfac. 2 (2015), https://doi.org/10.1002/admi.201400532.

[31] S. Olthof, K. Meerholz, Substrate-dependent electronic structure and film formation of MAPbI 3 perovskites, Sci. Rep. 7 (2017) 1–10, https://doi.org/10.1038/srep40267.

[32] E.M. Miller, Y. Zhao, C.C. Mercado, S.K. Saha, J.M. Luther, K. Zhu, V. Stevanović, C.L. Perkins, J. Van De Lagemaat, Substrate-controlled band positions in CH3NH3PbI3 perovskite films, Phys. Chem. Chem. Phys. 16 (2014) 22122–22130, https://doi.org/10.1039/c4cp03533j.

[33] Q. Wang, Y. Shao, H. Xie, L. Lyu, X. Liu, Y. Gao, J. Huang, Qualifying composition dependent p and n self-doping in CH3NH3PbI3, Appl. Phys. Lett. 105 (2014), https://doi.org/10.1063/1.4899051.

[34] A. Zohar, M. Kulbak, I. Levine, G. Hodes, A. Kahn, D. Cahen, What limits the open-circuit voltage of bromide perovskite-based solar cells? ACS Energy Lett. 4 (2019) 1–7, https://doi.org/10.1021/acsenergylett.8b01920.

[35] B. Dänekamp, C. Müller, M. Sendner, P.P. Boix, M. Sessolo, R. Lovrincic, H.J. Bolink, Perovskite-perovskite homojunctions via compositional doping, J. Phys. Chem. Lett. 9 (2018) 2770–2775, https://doi.org/10.1021/acs.jpclett.8b00964.

[36] P. Cui, D. Wei, J. Ji, H. Huang, E. Jia, S. Dou, T. Wang, W. Wang, M. Li, Planar p–n homojunction perovskite solar cells with efficiency exceeding 21.3, Nat. Energy 4 (2019) 150–159, https://doi.org/10.1038/s41560-018-0324-8.

[37] A. Zohar, I. Levine, S. Gupta, O. Davidson, D. Azulay, O. Millo, I. Balberg, G. Hodes, D. Cahen, What is the mechanism of MAPbI3 p-doping by I2? Insights from optoelectronic properties, ACS Energy Lett. 2 (2017) 2408–2414, https://doi.org/10.1021/acsenergylett.7b00698.

[38] Z. Su, Y. Chen, X. Li, S. Wang, Y. Xiao, The modulation of opto-electronic properties of CH3NH3PbBr3 crystal, J. Mater. Sci. Mater. Electron. 28 (2017) 11053–11058, https://doi.org/10.1007/s10854-017-6889-3.

[39] D. Song, P. Cui, T. Wang, D. Wei, M. Li, F. Cao, X. Yue, P. Fu, Y. Li, Y. He, B. Jiang, M. Trevor, Managing carrier lifetime and doping property of lead halide perovskite by postannealing processes for highly efficient perovskite solar cells, J. Phys. Chem. C 119 (2015) 22812–22819, https://doi.org/10.1021/acs.jpcc.5b06859.

[40] T. Liu, X. Zhao, J. Li, Z. Liu, F. Liscio, S. Milita, B.C. Schroeder, O. Fenwick, Enhanced control of self-doping in halide perovskites for improved thermoelectric performance, Nat. Commun. 10 (2019) 1–9, https://doi.org/10.1038/s41467-019-13773-3.

[41] A. Senocrate, T. Acartürk, G.Y. Kim, R. Merkle, U. Starke, M. Grätzel, J. Maier, Interaction of oxygen with halide perovskites, J. Mater. Chem. A. 6 (2018) 10847–10855, https://doi.org/10.1039/c8ta04537b.

[42] Y. Yang, X. Zou, Y. Pei, X. Bai, W. Jin, D. Chen, Effect of doping of NaI monovalent cation halide on the structural, morphological, optical and optoelectronic properties of MAPbI3 perovskite, J. Mater. Sci. Mater. Electron. 29 (2018) 205–210, https://doi.org/10.1007/s10854-017-7905-3.

[43] X. Bai, X. Zou, J. Zhu, Y. Pei, Y. Yang, W. Jin, D. Chen, Effect of Rb doping on modulating grain shape and semiconductor properties of MAPbI3 perovskite layer, Mater. Lett. 211 (2018) 328–330, https://doi.org/10.1016/j.matlet.2017.10.025.

[44] D. Regaldo, A. Bojar, S.P. Dunfield, P. Lopez-Varo, M. Frégnaux, V. Dufoulon, S.T. Zhang, J. Alvarez, J.J. Berry, J.B. Puel, P. Schulz, J.P. Kleider, On the equilibrium electrostatic potential and light-induced charge redistribution in halide perovskite structures, Prog. Photovoltaics Res. Appl. (2021), https://doi.org/10.1002/pip.3529.

[45] F. Peña-Camargo, J. Thiesbrummel, H. Hempel, A. Musiienko, V.M. Le Corre, J. Diekmann, J. Warby, T. Unold, F. Lang, D. Neher, M. Stolterfoht, Revealing the doping density in perovskite solar cells and its impact on device performance, Appl. Phys. Rev. 9 (2022), https://doi.org/10.1063/5.0085286.

[46] P. Lopez-Varo, J.A. Jiménez-Tejada, M. García-Rosell, S. Ravishankar, G. Garcia-Belmonte, I. Bisquert, O. Almora, Device physics of hybrid perovskite solar cells: theory and experiment, Adv. Energy Mater. 8 (2018), https://doi.org/10.1002/AENM.201702772.

[47] Q. Jiang, J. Tong, Y. Xian, R.A. Kerner, S.P. Dunfield, C. Xiao, R.A. Scheidt, D. Kuciauskas, X. Wang, M.P. Hautzinger, R. Tirawat, M.C. Beard, D.P. Fenning, J.J. Berry, B.W. Larson, Y. Yan, K. Zhu, Surface reaction for efficient and stable inverted perovskite solar cells, Nature (2022) 1–2, https://doi.org/10.1038/s41586-022-05268-x, 2022.

[48] B. Das, I. Aguilera, U. Rau, T. Kirchartz, Effect of doping, photodoping, and bandgap variation on the performance of perovskite solar cells, Adv. Opt. Mater. (2022), 2101947, https://doi.org/10.1002/adom.202101947.

[49] M. Burgelman, P. Nollet, S. Degrave, Modelling polycrystalline semiconductor solar cells, Thin Solid Films 361 (2000) 527–532, https://doi.org/10.1016/S0040-6090(99)00825-1.

[50] M. Burgelman, K. Decock, S. Khelifi, A. Abass, Advanced electrical simulation of thin film solar cells, Thin Solid Films 535 (2013) 296–301, https://doi.org/10.1016/j.tsf.2012.10.032.

[51] J. Diekmann, P. Caprioglio, M.H. Futscher, V.M. Le Corre, S. Reichert, F. Jaiser, M. Arvind, L.P. Toro, E. Gutierrez-Partida, F. Peña-Camargo, C. Deibel, B. Ehrler, T. Unold, T. Kirchartz, D. Neher, M. Stolterfoht, Pathways toward 30% efficient single-junction perovskite solar cells and the role of mobile ions, Sol. RRL. 5 (2021), https://doi.org/10.1002/solr.202100219.

[52] E. Raza, Z. Ahmad, F. Aziz, M. Asif, A. Ahmed, K. Riaz, J. Bhadra, N.J. Al-Thani, Numerical simulation analysis towards the effect of charge transport layers electrical properties on cesium based ternary cation perovskite solar cells performance, Sol. Energy 225 (2021) 842–850, https://doi.org/10.1016/j.solener.2021.08.008.

[53] T. Hellmann, M. Wussler, C. Das, R. Dachauer, I. El-Helaly, C. Mortan, T. Mayer, W. Jaegermann, The difference in electronic structure of MAPI and MASI perovskites and its effect on the interface alignment to the HTMs spiro-MeOTAD and CuI, J. Mater. Chem. C 7 (2019) 5324–5332, https://doi.org/10.1039/c8tc06332j.

[54] E. Karimi, S.M.B. Ghorashi, Investigation of the influence of different hole-transporting materials on the performance of perovskite solar cells, Optik 130 (2017) 650–658, https://doi.org/10.1016/j.ijleo.2016.10.122.

[55] Y. Raoui, H. Ez-Zahraouy, N. Tahiri, O. El Bounagui, S. Ahmad, S. Kazim, Performance analysis of MAPbI3 based perovskite solar cells employing diverse charge selective contacts: simulation study, Sol. Energy 193 (2019) 948–955, https://doi.org/10.1016/j.solener.2019.10.009.

[56] U. Mandadapu, Simulation and analysis of lead based perovskite solar cell using SCAPS-1D, Indian J. Sci. Technol. 10 (2017) 1–8, https://doi.org/10.17485/ijst/2017/v11i10/110721.

[57] C. Motta, F. El-Mellouhi, S. Sanvito, Charge carrier mobility in hybrid halide perovskites, Sci. Rep. 5 (2015), https://doi.org/10.1038/srep12746.

[58] C. Wehrenfennig, G.E. Eperon, M.B. Johnston, H.J. Snaith, L.M. Herz, C. Wehrenfennig, G.E. Eperon, M.B. Johnston, H.J. Snaith, L.M. Herz, High charge carrier mobilities and lifetimes in organolead trihalide perovskites, Adv. Mater. 26 (2014) 1584–1589, https://doi.org/10.1002/ADMA.201305172.

[59] G. Xosrovashvili, N.E. Gorji, Numerical analysis of TiO2/Cu2ZnSnS4 nano-structured PV using SCAPS-1D, J. Mod. Opt. 60 (2013) 936–940, https://doi.org/10.1080/09500340.2013.827252.

[60] T. Minemoto, M. Murata, Device modeling of perovskite solar cells based on structural similarity with thin film inorganic semiconductor solar cells, J. Appl. Phys. 116 (2014), https://doi.org/10.1063/1.4891982.

[61] K. Kalyanasundaram, Dye-sensitized Solar Cells (Fundamental Sciences: Chemistry), EPFL Press, 2010.

[62] S. Fonash, Solar Cell Device Physics, 2009.

[63] L. Schmidt-Mende, M. Grätzel, TiO2 pore-filling and its effect on the efficiency of solid-state dye-sensitized solar cells, Thin Solid Films 500 (2006) 296–301, https://doi.org/10.1016/j.tsf.2005.11.020.

[64] P.K. Patel, Device simulation of highly efficient eco-friendly CH3NH3SnI3 perovskite solar cell, Sci. Rep. 11 (2021) 1–11, https://doi.org/10.1038/s41598-021-82817-w.

[65] J. Jeong, M. Kim, J. Seo, H. Lu, P. Ahlawat, A. Mishra, Y. Yang, M.A. Hope, F.T. Eickemeyer, M. Kim, Y.J. Yoon, I.W. Choi, B.P. Darwich, S.J. Choi, Y. Jo, J.H. Lee, B. Walker, S.M. Zakeeruddin, L. Emsley, U. Rothlisberger, A. Hagfeldt, D.S. Kim, M. Grätzel, J.Y. Kim, Pseudo-halide anion engineering for α-FAPbI3 perovskite solar cells, Nature 592 (2021) 381–385, https://doi.org/10.1038/s41586-021-03406-5.

[66] J.J. Yoo, G. Seo, M.R. Chua, T.G. Park, Y. Lu, F. Rotermund, Y.K. Kim, C.S. Moon, N.J. Jeon, J.P. Correa-Baena, V. Bulović, S.S. Shin, M.G. Bawendi, J. Seo, Efficient perovskite solar cells via improved carrier management, Nature 590 (2021) 587–593, https://doi.org/10.1038/s41586-021-03285-w.

[67] M. Kim, J. Jeong, H. Lu, T.K. Lee, F.T. Eickemeyer, Y. Liu, I.W. Choi, S.J. Choi, Y. Jo, H.B. Kim, S.I. Mo, Y.K. Kim, H. Lee, N.G. An, S. Cho, W.R. Tress, S.M. Zakeeruddin, A. Hagfeldt, J.Y. Kim, M. Grätzel, D.S. Kim, Conformal quantum dot-SnO2 layers as electron transporters for efficient perovskite solar cells, Science 375 (2022) 302–306, https://doi.org/10.1126/science.abh1885.

[68] M. Saliba, T. Matsui, J.Y. Seo, K. Domanski, J.P. Correa-Baena, M.K. Nazeeruddin, S.M. Zakeeruddin, W. Tress, A. Abate, A. Hagfeldt, M. Grätzel, Cesium-containing triple cation perovskite solar cells: improved stability, reproducibility and high efficiency, Energy Environ. Sci. 9 (2016) 1989–1997, https://doi.org/10.1039/c5ee03874j.

[69] X. Li, D. Bi, C. Yi, J.D. Décoppet, J. Luo, S.M. Zakeeruddin, A. Hagfeldt, M. Grätzel, A vacuum flash-assisted solution process for high-efficiency large-area perovskite solar cells, Science 353 (2016) 58–62, https://doi.org/10.1126/science.aaf8060.

[70] P. Zhao, B.J. Kim, X. Ren, D.G. Lee, G.J. Bang, J.B. Jeon, W. Bin Kim, H.S. Jung, Antisolvent with an ultrawide processing window for the one-step fabrication

of efficient and large-area perovskite solar cells, Adv. Mater. 30 (2018), https://doi.org/10.1002/adma.201802763.

[71] N.-G. Zhang, Yong, Seul-Gi Kim, Donghwa Lee, Hyunjung Shin, Park, Bifacial stamping for high efficiency perovskite solar cells, Energy Environ. Sci. 12 (2019) 308−321, https://doi.org/10.1039/c8ee02730g.

[72] N. Ahn, D.-Y. Son, I.-H. Jang, S.M. Kang, M. Choi, N. Park, Highly reproducible perovskite solar cells with average Efficiency of 18.3% and best Efficiency of 19.7% fabricated via lewis base adduct of lead(II) iodide, J. Am. Chem. Soc. 137 (2015) 8696−8699, https://doi.org/10.1021/jacs.5b04930.

[73] N.K. Noel, S.N. Habisreutinger, B. Wenger, M.T. Klug, T.H. Maximilian, M.B. Johnston, R.J. Nicholas, D.T. Moore, H.J. Snaith, A low viscosity, low boiling point, clean solvent system for the rapid crystallisation of highly specular perovskite films, Energy Environ. Sci. 10 (2017) 145−152, https://doi.org/10.1039/c6ee02373h.

[74] J. Euvrard, Y. Yan, D.B. Mitzi, Electrical doping in halide perovskites, Nat. Rev. Mater. 6 (2021) 531−549, https://doi.org/10.1038/s41578-021-00286-z.

[75] C. Xiao, F. Zhang, Z. Li, S.P. Harvey, X. Chen, K. Wang, C.S. Jiang, K. Zhu, M. Al-Jassim, Inhomogeneous doping of perovskite materials by dopants from hole-transport layer, Matter 2 (2020) 261−272, https://doi.org/10.1016/j.matt.2019.10.005.

[76] S.P. Dunfield, A. Bojar, S. Cacovich, M. Frégnaux, T. Klein, R. Bramante, F. Zhang, D. Regaldo, V. Dufoulon, J.B. Puel, G. Teeter, J.M. Luther, M. Bouttemy, D. Nordlund, K. Zhu, D.T. Moore, M.F.A.M. van Hest, J.P. Kleider, J.J. Berry, P. Schulz, Carrier gradients and the role of charge selective contacts in lateral heterojunction all back contact perovskite solar cells, Cell Reports Phys. Sci. 2 (2021), https://doi.org/10.1016/j.xcrp.2021.100520.

[77] N.K. Noel, S.N. Habisreutinger, B. Wenger, Y.H. Lin, F. Zhang, J.B. Patel, A. Kahn, M.B. Johnston, H.J. Snaith, Elucidating the role of a tetrafluoroborate-based ionic liquid at the n-type oxide/perovskite interface, Adv. Energy Mater. 10 (2020), https://doi.org/10.1002/aenm.201903231.

[78] M.L.C.E.E. Perry, J.G. Labram, N.:R. Venkatesan, H. Nakayama, N-type surface doping of MAPbI3 via charge transfer from small molecules, Adv. Electron. Mater. 4 (2018), https://doi.org/10.1002/aelm.201800087.

[79] H. Chen, Y. Zhan, G. Xu, W. Chen, S. Wang, M. Zhang, Y. Li, Y. Li, Organic N-type molecule: managing the electronic states of bulk perovskite for high-performance photovoltaics, Adv. Funct. Mater. 30 (2020), https://doi.org/10.1002/adfm.202001788.

[80] N.K. Noel, S.N. Habisreutinger, A. Pellaroque, F. Pulvirenti, B. Wenger, F. Zhang, Y.H. Lin, O.G. Reid, J. Leisen, Y. Zhang, S. Barlow, S.R. Marder, A. Kahn, H.J. Snaith, C.B. Arnold, B.P. Rand, Interfacial charge-transfer doping of metal halide perovskites for high performance photovoltaics, Energy Environ. Sci. 12 (2019) 3063−3073, https://doi.org/10.1039/c9ee01773a.

[81] Arramel, H. Pan, A. Xie, S. Hou, X. Yin, C.S. Tang, N.T. Hoa, M.D. Birowosuto, H. Wang, C. Dang, A. Rusydi, A.T.S. Wee, J. Wu, Surface molecular doping of all-inorganic perovskite using zethrenes molecules, Nano Res. 12 (2019) 77−84, https://doi.org/10.1007/s12274-018-2183-9.

[82] Q. Jiang, Z. Ni, G. Xu, Y. Lin, P.N. Rudd, R. Xue, Y. Li, Y. Li, Y. Gao, J. Huang, Interfacial molecular doping of metal halide perovskites for highly efficient solar cells, Adv. Mater. 32 (2020), https://doi.org/10.1002/adma.202001581.

[83] W.Q. Wu, Q. Wang, Y. Fang, Y. Shao, S. Tang, Y. Deng, H. Lu, Y. Liu, T. Li, Z. Yang, A. Gruverman, J. Huang, Molecular doping enabled scalable blading of efficient hole-transport-layer-free perovskite solar cells, Nat. Commun. 9 (2018) 1−8, https://doi.org/10.1038/s41467-018-04028-8.

[84] E.A. Gaulding, J. Hao, H.S. Kang, E.M. Miller, S.N. Habisreutinger, Q. Zhao, A. Hazarika, P.C. Sercel, J.M. Luther, J.L. Blackburn, Conductivity tuning via doping with electron donating and withdrawing molecules in perovskite CsPbI3 nano-crystal films, Adv. Mater. 31 (2019), https://doi.org/10.1002/adma.201902250.

[85] S. Tan, I. Yavuz, M.H. Weber, T. Huang, C.H. Chen, R. Wang, H.C. Wang, J.H. Ko, S. Nuryyeva, J. Xue, Y. Zhao, K.H. Wei, J.W. Lee, Y. Yang, Shallow iodine defects accelerate the degradation of α-phase formamidinium perovskite, Joule 4 (2020) 2426−2442, https://doi.org/10.1016/J.JOULE.2020.08.016.